Open access • Journal Article • DOI:10.1080/02726340701272139

Conductance Between Two Strip Electrodes on a Conducting Ground with a Nearby Tunnel — Source link

Robert W. Scharstein, Paul M. Goggans

Institutions: University of Alabama, University of Mississippi

Published on: 01 Jun 2007 - Electromagnetics (Taylor & Francis Group)

Topics: Cylindrical coordinate system

This is the authors' AmS-TeX manuscript. The published paper appears in the journal *Electromagnetics,* vol 27, no 4, pp. 183–194, May 2007.

Conductance Between Two Strip Electrodes on a Conducting Ground with a Nearby Tunnel

ROBERT W. SCHARSTEIN

Electrical Engineering Department
University of Alabama
Tuscaloosa, Alabama, USA

PAUL M. GOGGANS

Electrical Engineering Department
University of Mississippi
University, Mississippi, USA

Abstract The zero-frequency problem of a pair of perfectly-conducting strip electrodes lying on an imperfectly conducting half-space and perturbed by the presence of a non-conductive cylindrical void or tunnel is analyzed. A conformal mapping transforms all of the pertinent boundaries in the potential problem to simple coordinate surfaces in a single cylindrical coordinate frame. Coupled integral equations for the normal electric current density on each strip are numerically solved using the moment method. The effect upon the circuit resistance of various sized subsurface tunnels at arbitrary locations is now easily calculable.

Keywords conformal mapping, integral equation, Laplace's equation, static solution

Direct correspondence to:

Robert W. Scharstein
Electrical Engineering Department
University of Alabama
317 Houser Hall
Tuscaloosa, AL 35487-0286

phone 205-348-1761
fax 205-348-6959
e-mail: `rscharst@bama.ua.edu`

Introduction

The detection and localization of voids and tunnels in soils is a problem of considerable practical application. A simple electrical measurement apparatus composed of two electrodes placed on the soil surface and held a fixed distance apart can yield data relevant to this detection and localization problem. During data collection the conductance between the electrodes is recorded as the electrodes are moves across the soil surface. Variation in the measured conductance indicates the potential presence of a subsurface void or tunnel while the shape of the conductance versus distance curve provides clues about the location of the void or tunnel.

A two-dimensional boundary value problem is proposed as a simple model to understand and quantify the perturbative effect of a nonconductive void or tunnel on the conductance between a pair of electrodes placed on the surface of a conducting ground or half-space. The axis of the buried tunnel runs parallel to the strip electrodes and disturbs some fraction of the electric current that flows in the conductive half-space. The DC current density that flows in the conducting medium is written as the gradient of a harmonic function ψ, subject to Neumann boundary conditions on the interfaces with the nonconductive (air in the motivating application) media. A conformal mapping transforms all of the boundaries to coaxial circular arcs in cylindrical polar coordinates. Coupled integral equations for the unknown normal current density (normal derivative of ψ) are written in terms of a modified Green's function that is constructed in the cylindrical coordinates. The Neumann compatibility condition is assured by the explicit inclusion of an image source at infinity in the original z-plane, which is mapped to the point $\zeta = 1 + i0$ on the image of the air/ground interface. An easily implemented moment method solution uses pulse expansion and point matching. Resultant variations in net strip conductance with tunnel size and proximity to the strips reveal that the effect of the tunnel is relatively small. A true physical configuration of three-dimensional electrodes will certainly differ from the two-dimensional idealization studied here, but the two-dimensional results give an indica-

tion of the magnitude of the change in conductance due to a nearby void. Additionally, the theoretical value of the static boundary value problem and its solution are rather independent of and are not limited to the motivating application.

Potential Problem and Conformal Mapping

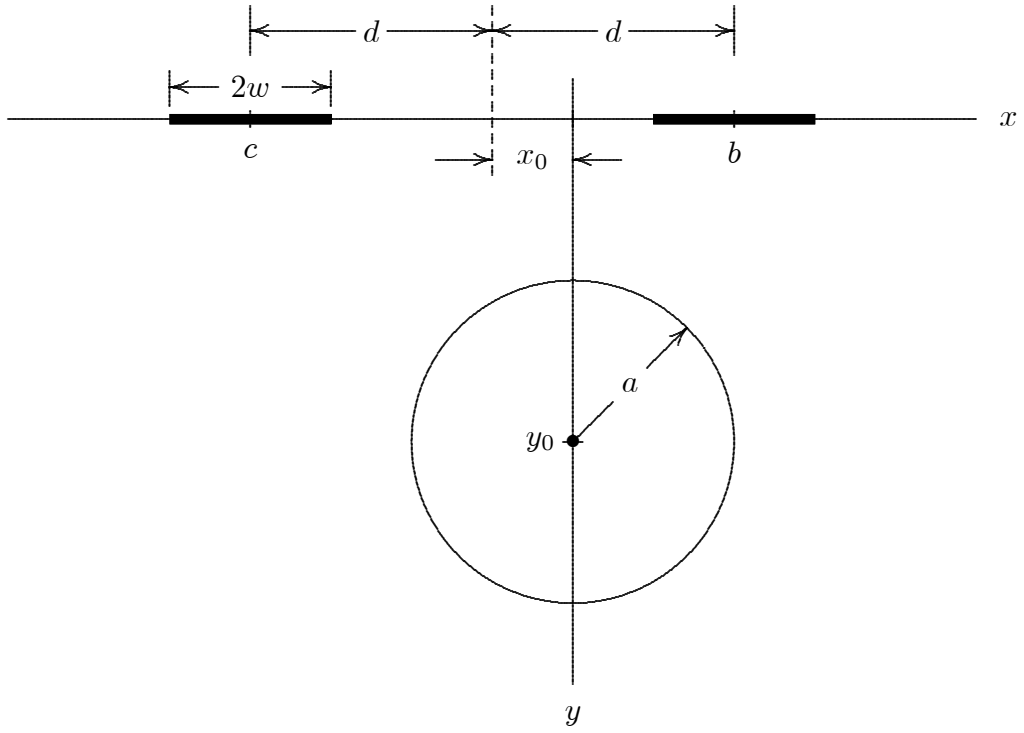

FIG. 1. Circular Inhomogeneity Below a Pair of Strip Electrodes

The two-dimensional potential problem depicted in Fig. 1 consists of a pair of perfectly conducting strip electrodes lying on a half-space of conductivity σ (℧/m). The strips are each of width $2w$ and their center-to-center separation is $2d$. The circular void or tunnel of radius a has zero conductivity. The center of the circular tunnel is displaced by x_0 from the midpoint between the two electrodes, and this center is at a depth y_0 below the earth/air interface. The x-coordinates of the centers of the two electrodes are

$$b = d - x_0 \qquad \text{and} \qquad c = b - 2d \tag{1}$$

and are labeled in Fig. 1. The electrode C_1 on the right (with center at $x = b$) is held to a fixed potential V_1 (V) and the electrode C_2 on the left (with center at $x = c$) is maintained at the potential V_2 (V), causing an electric current density

$$\vec{J} = -\sigma \nabla \psi \tag{2}$$

to flow in the conducting earth. Therefore, we seek a harmonic potential $\psi(x, y)$ that is the solution to Laplace's equation in the half-space

$$\nabla^2 \psi(x, y) = 0 \qquad (-\infty < x < \infty, \quad y \geq 0), \tag{3}$$

subject to Neumann boundary conditions $\partial\psi/\partial\nu = 0$ on the circular boundary and on the portion of the $y = 0$ plane not covered by the strips, and with the prescribed Dirichlet conditions $\psi = V_1$ on C_1 and $\psi = V_2$ on C_2.

The solution to this boundary value problem is constructed via a conformal mapping (Henrici, 1974) that places both boundaries in a consistent coordinate system. The auxiliary parameters

$$s = \sqrt{y_0^2 - a^2} \qquad \text{and} \qquad R = \frac{a}{y_0 + s} \tag{4}$$

appear in the bilinear transformation

$$\zeta = \frac{z - is}{z + is} \qquad \Longleftrightarrow \qquad z = is\frac{1 + \zeta}{1 - \zeta} \tag{5}$$

between the physical $z = x + iy$ and mapped $\zeta = \xi + i\eta = re^{i\phi}$ planes.

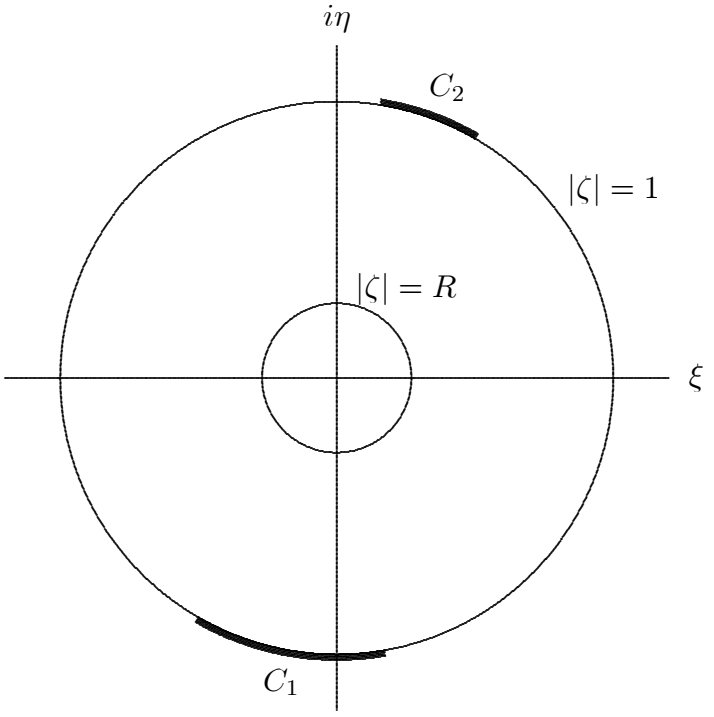

FIG. 2. Complex $\zeta = \xi + i\eta$ Plane

The entire earth-to-ground interface (the $y = 0$ plane in Fig. 1) is mapped to the unit circle in Fig. 2 and the boundary of the tunnel is mapped to the coaxial circle of radius R. The images of the electrodes C_1 and C_2 are arcs on the unit circle. The potential problem in the ζ plane is therefore

$$\nabla^2 \psi(r, \phi) = 0 \qquad (R \leq r \leq 1) \tag{6}$$

with the mixed boundary conditions

$$\frac{\partial}{\partial r}\psi(R, \phi) = 0 \tag{7}$$

$$\psi(\zeta) = V_2 \quad (\zeta \in C_2) \tag{8}$$

$$\psi(\zeta) = V_1 \quad (\zeta \in C_1) \tag{9}$$

$$\frac{\partial}{\partial r}\psi(\zeta) = 0 \quad (|\zeta| = 1 \text{ and } \zeta \notin C_1, C_2). \tag{10}$$

The total current in Fig. 1 leaving strip C_1 (per unit length in the infinite dimension) is

$$I_1 = \int_{C_1} \vec{J} \cdot \hat{\nu}\, d\ell = -\sigma \int_{C_1} \frac{\partial \psi}{\partial \nu}\, d\ell. \tag{11}$$

Green's Function and Neumann Compatibility

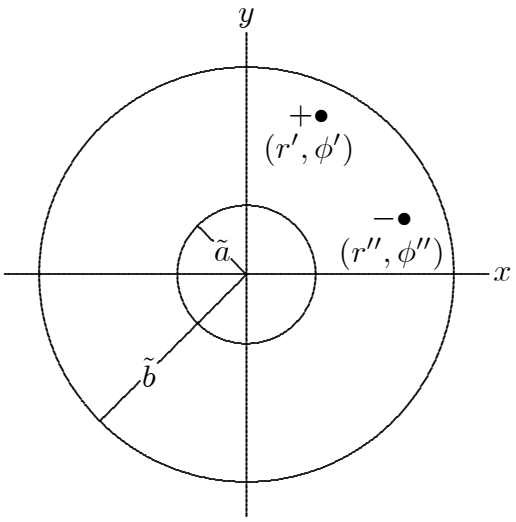

FIG. 3. Coaxial Region and Pair of Point Sources

The usual Neumann compatibility requirement (Courant and Hilbert, 1962) is dictated by Gauss' law

$$\iint_S \nabla^2 \psi\, ds = \oint_C \frac{\partial \psi}{\partial \nu}\, d\ell. \tag{12}$$

If $\partial\psi/\partial\nu = 0$ on the entire closed boundary C of the finite region S in Fig. 3, then the total source strength $\nabla^2\psi$ must integrate to zero over S. Therefore, a positive source singularity in the interior region S at (r', ϕ') is accompanied by a negative source of the same magnitude, located at some other point (r'', ϕ''). The required fundamental solution or Green's function is denoted by $G^{(2)}$, where the superscript 2 calls attention to the presence of the *pair* of sources. Standard Fourier series and separation-of-variables (Barton, 1989) give the solution to Poisson's equation

$$\nabla^2 G^{(2)}(r, \phi; r', \phi'; r'', \phi'') = -\frac{1}{r}\delta(r - r')\delta(\phi - \phi') + \frac{1}{r}\delta(r - r'')\delta(\phi - \phi'') \tag{13}$$

subject to Neumann conditions

$$\frac{\partial}{\partial r} G^{(2)}(r,\phi;r',\phi';r'',\phi'')\bigg|_{r=\tilde{a},\tilde{b}} = 0 \tag{14}$$

on each of the hard circular boundaries, as

$$\begin{aligned}
&G^{(2)}(r,\phi;r',\phi';r'',\phi'') \\
&\quad = -\frac{1}{4\pi}\ln\left[r^2+r'^2-2rr'\cos(\phi-\phi')\right] \\
&\qquad + \frac{1}{2\pi}\sum_{n=1}^{\infty}\left[\left(\frac{r'r}{\tilde{b}^2}\right)^n + \left(\frac{\tilde{a}^2 r}{\tilde{b}^2 r'}\right)^n + \left(\frac{\tilde{a}^2}{r'r}\right)^n + \left(\frac{\tilde{a}^2 r'}{\tilde{b}^2 r}\right)^n\right]\frac{\cos n(\phi-\phi')}{n\left[1-(\tilde{a}/\tilde{b})^{2n}\right]} \\
&\qquad + \frac{1}{4\pi}\ln\left[r^2+r''^2-2rr''\cos(\phi-\phi'')\right] \\
&\qquad - \frac{1}{2\pi}\sum_{n=1}^{\infty}\left[\left(\frac{r''r}{\tilde{b}^2}\right)^n + \left(\frac{\tilde{a}^2 r}{\tilde{b}^2 r''}\right)^n + \left(\frac{\tilde{a}^2}{r''r}\right)^n + \left(\frac{\tilde{a}^2 r''}{\tilde{b}^2 r}\right)^n\right]\frac{\cos n(\phi-\phi'')}{n\left[1-(\tilde{a}/\tilde{b})^{2n}\right]}.
\end{aligned} \tag{15}$$

When both the positive and negative sources lie on the outer boundary, as well as the field point, that is with $r = r' = r'' = \tilde{b}$, then the $G^{(2)}$ simplifies according to

$$\begin{aligned}
&G^{(2)}(\tilde{b},\phi;\tilde{b},\phi';\tilde{b},\phi'') \\
&\quad = \frac{1}{2\pi}\sum_{n=1}^{\infty}\frac{1}{n}\left[1+\frac{1+3(\tilde{a}/\tilde{b})^{2n}}{1-(\tilde{a}/\tilde{b})^{2n}}\right]\left[\cos n(\phi-\phi')-\cos n(\phi-\phi'')\right] \\
&\quad = \frac{1}{2\pi}\sum_{n=1}^{\infty}\frac{1}{n}\left[\cos n(\phi-\phi')-\cos n(\phi-\phi''\right] \\
&\qquad\qquad + \frac{2}{\pi}\sum_{n=1}^{\infty}\frac{(\tilde{a}/\tilde{b})^{2n}}{n[1-(\tilde{a}/\tilde{b})^{2n}]}\left[\cos n(\phi-\phi')-\cos n(\phi-\phi''\right] \\
&\quad = -\frac{1}{2\pi}\ln\left|\sin\tfrac{1}{2}(\phi-\phi')\right| + \frac{1}{2\pi}\ln\left|\sin\tfrac{1}{2}(\phi-\phi'')\right| \\
&\qquad\qquad + \frac{2}{\pi}\sum_{n=1}^{\infty}\frac{(\tilde{a}/\tilde{b})^{2n}}{n[1-(\tilde{a}/\tilde{b})^{2n}]}\left[\cos n(\phi-\phi')-\cos n(\phi-\phi''\right].
\end{aligned} \tag{16}$$

Boundary Value Problem for the Coaxial Region

Returning to the conformal map of Fig. 2, the specialization $\tilde{a} = R$ and $\tilde{b} = 1$ is applied to the Green's function for the annulus of Fig. 3. An integral equation statement of the

boundary value problem is formulated using Green's second identity

$$\iint_S \left[G(\vec{r},\vec{r}\,')\nabla^2\psi(\vec{r}) - \psi(\vec{r})\nabla^2 G(\vec{r},\vec{r}\,')\right]\, ds \\ = \oint_C \left[G(\vec{r},\vec{r}\,')\frac{\partial}{\partial\nu}\psi(\vec{r}) - \psi(\vec{r})\frac{\partial}{\partial\nu}G(\vec{r},\vec{r}\,')\right]\, d\ell, \tag{17}$$

where $\hat{\nu}$ is the outward normal on the boundary C of the finite region S. The solution of the original statement of the boundary value problem given in (6)-(10) is now constructed with the aid of the "double-source" Green's function from above

$$\nabla^2 G^{(2)}(\vec{r},\vec{r}\,',\vec{r}\,'') = -\delta(\vec{r}-\vec{r}\,') + \delta(\vec{r}-\vec{r}\,'') \tag{18}$$

that satisfies Neumann conditions

$$\frac{\partial}{\partial r}G^{(2)} = 0 \tag{19}$$

on the entire boundary $r = R, 1$. As both of the points r' and r'' approach the outer circle $|\zeta| = 1$, the appropriate limit of (17) reveals

$$\tfrac{1}{2}\psi(\vec{r}\,') = \oint_C G^{(2)}(\vec{r},\vec{r}\,',\vec{r}\,'')\frac{\partial}{\partial r}\psi(\vec{r})\, d\ell \,+\, \tfrac{1}{2}\psi(\vec{r}\,''). \tag{20}$$

With $\tilde{a} = R$ and $\tilde{b} = 1$ and $\phi'' = 0$, the required Green's function (16) is

$$G^{(2)}(\phi,\phi') = -\frac{1}{2\pi}\ln\left|\sin\tfrac{1}{2}(\phi-\phi')\right| + \frac{1}{2\pi}\ln\left|\sin\tfrac{1}{2}\phi\right| \\ + \frac{2}{\pi}\sum_{n=1}^{\infty}\frac{R^{2n}}{n[1-R^{2n}]}\left[\cos n(\phi-\phi') - \cos n\phi\right]. \tag{21}$$

The potential at infinity is $\psi(\vec{r}\,'') = 0$ consistent with the zero total source strength; therefore this monopole contribution at infinity is zero. For $j = 1, 2$ the integral equation for $\partial\psi_j/\partial r$ is

$$2\int_{C_1} G^{(2)}(\phi,\phi')\frac{\partial}{\partial r}\psi_1(\phi)\, d\phi + 2\int_{C_2} G^{(2)}(\widetilde{\phi},\phi')\frac{\partial}{\partial r}\psi_2(\widetilde{\phi})\, d\widetilde{\phi} = V_j \qquad (\phi' \in C_j) \tag{22}$$

where the tilde on the C_2 coordinate distinguishes between the two contours C_1 and C_2 of different sizes. The end-points of the arcs C_1 and C_2 are defined according to

$$\phi \in C_1 \quad\Longrightarrow\quad \Phi_1 < \phi < \Phi_2, \qquad \widetilde{\phi} \in C_2 \quad\Longrightarrow\quad \Phi_3 < \widetilde{\phi} < \Phi_4. \tag{23}$$

Piecewise Constant Approximation with Collocation

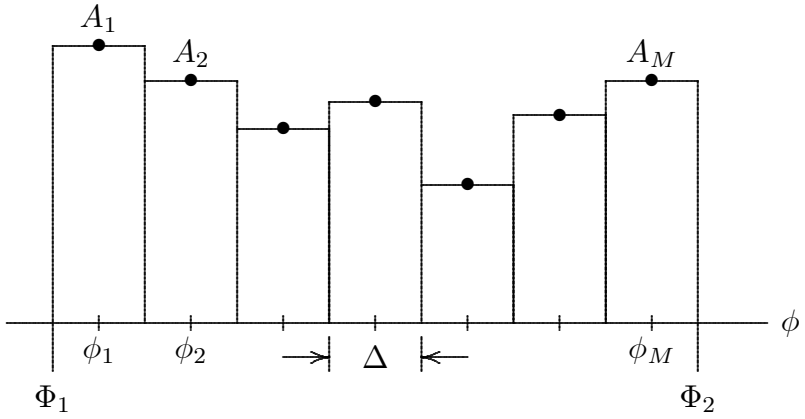

FIG. 4. Piecewise Constant Approximation in Terms of Pulse Basis

A conceptually simple and easily implemented moment method solution to the coupled integral equations (22) proceeds by expanding the normal derivative of the potential on strip C_1

$$\frac{\partial}{\partial r}\psi_1(\phi) = \sum_{m=1}^{M} A_m \Pi\left(\frac{\phi - \phi_m}{\Delta}\right) \tag{24}$$

in terms of the standard rectangular pulse

$$\Pi(t) = \begin{cases} 1, & |t| < 1/2 \\ 0, & |t| > 1/2. \end{cases} \tag{25}$$

The strip C_1 is divided into M segments of equal width

$$\Delta = \frac{\Phi_2 - \Phi_1}{M} \tag{26}$$

and the center of the mth segment has angular coordinate

$$\phi_m = \Phi_1 + (m - 1/2)\Delta. \tag{27}$$

Similarly, let

$$\frac{\partial}{\partial r}\psi_2(\widetilde{\phi}) = \sum_{n=1}^{N} B_n \Pi\left(\frac{\widetilde{\phi} - \widetilde{\phi}_n}{\widetilde{\Delta}}\right) \tag{28}$$

$$\widetilde{\Delta} = \frac{\Phi_4 - \Phi_3}{N} \tag{29}$$

$$\widetilde{\phi}_n = \Phi_3 + (n - 1/2)\widetilde{\Delta} \tag{30}$$

denote the corresponding discretization of strip C_2. Collocation or point matching at the points $\phi' = \phi_p$ $(p = 1, 2, \ldots, M)$ gives

$$2\sum_{m=1}^{M} A_m \int_{\phi_m - \Delta/2}^{\phi_m + \Delta/2} G^{(2)}(\phi, \phi_p)\, d\phi + 2\sum_{n=1}^{N} B_n \int_{\widetilde{\phi}_n - \widetilde{\Delta}/2}^{\widetilde{\phi}_n + \widetilde{\Delta}/2} G^{(2)}(\widetilde{\phi}, \phi_p)\, d\widetilde{\phi} = V_1, \tag{31}$$

and for $\phi' = \widetilde{\phi}_q$ $(q = 1, 2, \ldots, N)$

$$2\sum_{m=1}^{M} A_m \int_{\phi_m - \Delta/2}^{\phi_m + \Delta/2} G^{(2)}(\phi, \widetilde{\phi}_q)\, d\phi + 2\sum_{n=1}^{N} B_n \int_{\widetilde{\phi}_n - \widetilde{\Delta}/2}^{\widetilde{\phi}_n + \widetilde{\Delta}/2} G^{(2)}(\widetilde{\phi}, \widetilde{\phi}_q)\, d\widetilde{\phi} = V_2. \tag{32}$$

The efficient computation of the elements in these coupled matrix equations

$$\begin{aligned} \sum_{m=1}^{M} A_m W_{pm} + \sum_{n=1}^{N} B_n X_{pn} &= V_1 \qquad (p = 1, 2, \ldots, M) \\ \sum_{m=1}^{M} A_m Y_{qm} + \sum_{n=1}^{N} B_n Z_{qn} &= V_2 \qquad (q = 1, 2, \ldots, N) \end{aligned} \tag{33}$$

is accomplished with a combination of analytic integration of the simple logarithmic singularities and high-order Gaussian quadrature applied to the regular parts.

For example, the element

$$\begin{aligned} W_{pm} &= 2 \int_{\phi_m - \Delta/2}^{\phi_m + \Delta/2} G^{(2)}(\phi, \phi_p)\, d\phi \\ &= -\frac{1}{\pi} \int_{\phi_m - \Delta/2}^{\phi_m + \Delta/2} \ln\left|\sin\tfrac{1}{2}(\phi - \phi_p)\right|\, d\phi + \frac{1}{\pi} \int_{\phi_m - \Delta/2}^{\phi_m + \Delta/2} \ln\left|\sin\tfrac{1}{2}\phi\right|\, d\phi \\ &\quad + \frac{4}{\pi} \sum_{k=1}^{\infty} \frac{R^{2k}}{k[1 - R^{2k}]} \int_{\phi_m - \Delta/2}^{\phi_m + \Delta/2} [\cos k(\phi - \phi_p) - \cos k\phi]\, d\phi \end{aligned} \tag{34}$$

requires the evaluation of the integral

$$S_1(m, p) = \int_{\phi_m - \Delta/2}^{\phi_m + \Delta/2} \ln\left|\sin\tfrac{1}{2}(\phi - \phi_p)\right|\, d\phi = 2 \int_{(m-p-1/2)\Delta/2}^{(m-p+1/2)\Delta/2} \ln|\sin x|\, dx. \tag{35}$$

The diagonal case is

$$\begin{aligned} S_1(m,m) &= 4\int_0^{\Delta/4} \ln\sin x\, dx \\ &= 4\int_0^{\Delta/4} \left[\ln x - \frac{x^2}{6} - \frac{x^4}{180} + \ldots\right] dx \\ &= \Delta\ln(\Delta/4) - \Delta - \frac{\Delta^3}{288} - \frac{\Delta^5}{230,400} + \ldots \end{aligned} \tag{36}$$

and a related integral

$$S_2(m) = \int_{\phi_m-\Delta/2}^{\phi_m+\Delta/2} \ln\left|\sin\tfrac{1}{2}\phi\right|\, d\phi \tag{37}$$

also appears in the final form

$$W_{pm} = -\frac{1}{\pi}S_1(m,p)+\frac{1}{\pi}S_2(m)+\frac{8}{\pi}\sum_{k=1}^{\infty}\frac{R^{2k}}{k^2[1-R^{2k}]}\sin(\tfrac{1}{2}k\Delta)\Big\{\cos[k(m-p)\Delta]-\cos(k\phi_m)\Big\}. \tag{38}$$

The elements of the other three coefficient matrices in (33) are all similar, but different enough to require separate numerics; the details are not as interesting as the results.

The solution of matrix equation (33) gives the coefficients A_m in (24) required for the current density on strip C_1, as well as the B_n in (28) that represent the current density on strip C_2. The total current (11) flowing out from each strip is now

$$I_1 = -\sigma\Delta\sum_{m=1}^{M} A_m \tag{39}$$

and

$$I_2 = -\sigma\widetilde{\Delta}\sum_{n=1}^{N} B_n, \tag{40}$$

and the circuit conductance measured between the perfectly conducting strips held at potentials V_1 and V_2, respectively, is

$$G = \frac{I_1 - I_2}{2(V_1 - V_2)}. \tag{41}$$

Results

The resultant equipotentials of Figs. 5 and 6 depict a representative geometry where the center-to-center strip spacing is $2d = 4$, the strips are each of width $2w = 1$, and the center of a tunnel of radius $a = 2$ is located at a depth of $y_0 = 3$ and a midpoint displacement of $x_0 = 1$. The tunnel center is the origin of the ζ-plane of Fig. 5, where the images of the equal-width strips in the z-plane of Fig. 6 have different arc lengths. The strips of equal width in the physical z-plane of Fig. 6 have conformal images of different arc length in the mapped ζ-plane of Fig. 5. This is because the ζ-plane measures everything relative to its origin, which is the center of the tunnel. Fig. 7 presents a family of curves that show how the normalized conductance (per unit length) between one pair of strips ($2d = 4$ and $2w = 1$) varies when tunnels of different radii are moved relative to the midpoint between the electrodes. The depth used is $y_0 = 3$ and four tunnel sizes are considered: $a = 2.5, 2.0, 1.5$, and 1.0. The use of $N = 10$ and $M = 10$ piecewise constant basis functions provides satisfactory "numerical" or "self" convergence in this case.

In the absence of a tunnel, integration of the exact surface flux from an obvious scaling of Sneddon's result (Sneddon, 1966) gives

$$G/\sigma = \frac{\mathbf{K}\left(\sqrt{1 - r_0^2}\right)}{\mathbf{K}(r_0)} \tag{42}$$

in terms of the complete elliptic integral (Armitage and Eberlein, 2006), where

$$r_0 = \frac{d - w}{d + w}. \tag{43}$$

This "no tunnel" value appears as the dashed curve in Fig. 7, and is a logical standard with which to compare the perturbed conductances. The curves in Fig. 7 exhibit the required continuity and evenness about $x_0 = 0$ and approach the "no tunnel" value as $a \to 0$ or $x_0 \to \infty$.

The smoothness and relatively weak dependence upon x_0 of the G/σ curves are manifestations of the maximum principle for harmonic functions. The bottom curve in Fig. 7

depicts a relatively large tunnel (compared to the strip separation $2d = 4$) having a diameter $2a = 5$ and buried so that its top is at the shallow depth $y_0 - a = 1/2$. This large void decreases the conductance to about 50% of the "no tunnel" value, when $x_0| \lesssim 3$. Naturally, smaller or deeper obstacles have less effect on the circuit, as confirmed by the remaining curves in Fig. 7.

Conclusions

Laplace's equation is numerically solved in the conformally-mapped geometry where a pair of strip electrodes on a conducting half-space are influenced by a nearby circular region of zero conductivity. An integral of the solution gives the variation of the global conductance measured between the two electrodes as a function of the location and size of the circular inhomogeneity.

References

Armitage, J.V., and W.F. Eberlein. 2006. *Elliptic Functions.* Cambridge: Cambridge University Press., p. 212.

Barton, G. 1989. *Elements of Green's Functions and Propagation: Potentials, Diffusions, and Waves.* Oxford: Oxford University Press., pp. 413–417.

Courant, R., and D. Hilbert. 1962. *Methods of Mathematical Physics Vol II.* New York: Wiley., p. 252.

Henrici, P. 1974. *Applied and Computational Complex Analysis Vol 1.* New York: Wiley., Chapter 5.

Sneddon, I.N. 1966. *Mixed Boundary Value Problems in Potential Theory.* Amsterdam: North-Holland., p. 267.

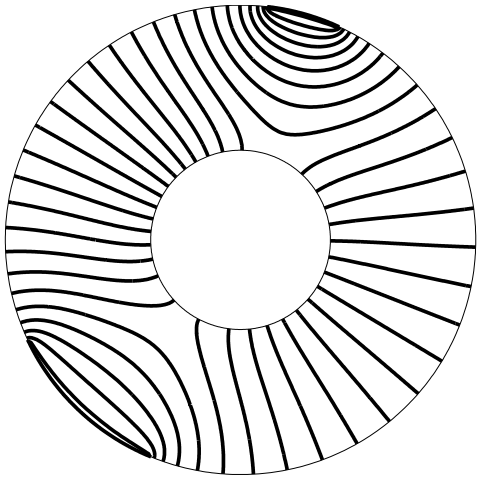

FIG. 5. Equipotentials in the ζ Plane
Geometry: $x_0 = 1$, $y_0 = 3$, $a = 2$, $d = 2$, $w = 0.5$

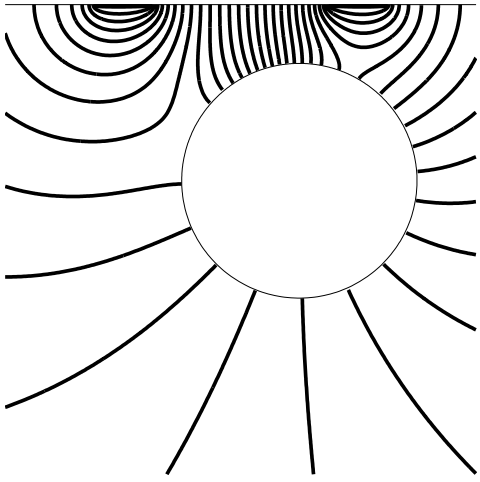

FIG. 6. Equipotentials in the z Plane
Geometry: $x_0 = 1$, $y_0 = 3$, $a = 2$, $d = 2$, $w = 0.5$

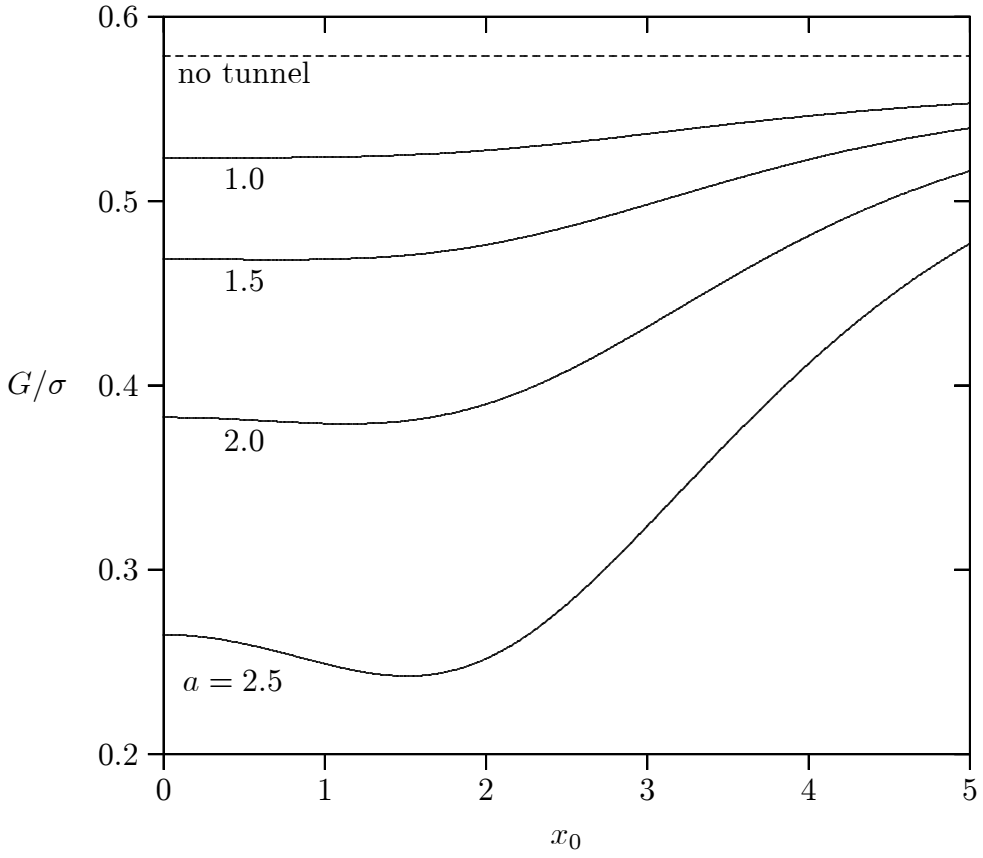

FIG. 7. Normalized Conductance per Unit Length
$y_0 = 3$, $d = 2$, $w = 0.5$, $N = M = 10$

List of Figure Captions

1. Circular Inhomogeneity Below a Pair of Strip Electrodes

2. Complex $\zeta = \xi + i\eta$ Plane

3. Coaxial Region and Pair of Point Sources

4. Piecewise Constant Approximation in Terms of Pulse Basis

5. Equipotentials in the ζ Plane
   Geometry: $x_0 = 1$, $y_0 = 3$, $a = 2$, $d = 2$, $w = 0.5$

6. Equipotentials in the z Plane
   Geometry: $x_0 = 1$, $y_0 = 3$, $a = 2$, $d = 2$, $w = 0.5$

7. Normalized Conductance per Unit Length
   $y_0 = 3$, $d = 2$, $w = 0.5$, $N = M = 10$